

**SYNTHESIS AND CHARACTERIZATION OF MgO-Cr₂O₃-ZTA CUTTING
TOOL MATERIAL**

by

AHMAD ZAHIRANI AHMAD AZHAR

Thesis submitted in fulfilment of the requirements

for the degree of

Doctor of Philosophy

January 2013

Author's declaration

I hereby declare that I have conducted, completed the research work and written the dissertation entitled “SYNTHESIS AND CHARACTERIZATION OF MgO-Cr₂O₃-ZTA CUTTING TOOL MATERIAL”. I also declare that it has not been previously submitted for the award of any degree or diploma or other similar title of this or any other examining body or university.

Signature of candidate:

Name of candidate: Ahmad Zahirani Ahmad Azhar

Date:

Witness by:

Signature of witness (main supervisor):

Name: Professor Hj. Zainal Arifin b. Hj. Ahmad

Date:

Acknowledgement

Praise to Allah, the Cherisher and Sustainer of the worlds, for making this thesis a reality. I wish to express my gratitude to my main supervisor, Prof. Dr. Hj. Zainal Arifin Hj. Ahmad, for the inspiration, motivation and professionally guiding me to successfully complete my research work. I would like to also thank him for providing me with outstanding research facilities and numerous technical discussions which I found to be very valuable to my research. His constant enthusiasm and insightfulness will be a model for my career. I would like to express my great appreciation to Prof. Dr. Mani Maran a/l Ratnam for his contribution on the co-supervision and valuable suggestions for this research and thesis. I would also like to thank Assoc. Prof. Dr. Hasmaliza Mohamad for her co-supervision in my research. Next, I would like to convey my special thanks to dean, Professor Ahmad Fauzi b. Mohd Noor, Deputy Deans, lecturers and all staffs of the School of Materials and Mineral Resources Engineering, Universiti Sains Malaysia (USM), for their kind assistant and supports. Without their kind cooperation, this study may not be completed on time. I gratefully acknowledge the USM Fellowship Scheme for their sponsorship throughout my study. My gratitude to Mr. Abdul Rashid, Mr. Mohd. Shahid, Mr. Khairi, Mr. Mokhtar, Mr. Farid, and Mr. Sharul Ami for their experimental and technical assistant. My time in USM wouldn't be pleasant without accompany of friends and colleagues; Dr. Azam, Dr. Zaky, Dr. Warikh, Dr. Shah Rizal, Dr. Farhad, Dr. Hazman, Dr. Saidatul Akma, Dr. Banjuraizah, Dr. Al-Amin, Dr. Hazman, Dr. Julie, Dr. Nor Azam, Dr. Norazharudin, Mohdarif, Nik Akmar, Md Nor, Fahmin, Azwadi, Johari, Faris and Rashid. I would like to thank my beloved wife, Nurdina Abd Kadir, for her endless love and support for encouraging me in all my efforts to this day. Lastly, my special and deepest appreciation and thanks go to

both my parents, Ahmad Azhar Mohamad and Norul Aini Ishak. Their constant support, encouragement gives warmth and strength to me. They always are there to share my success as well during sad and down time. Their inspiration, understanding, patience and support help me to complete this thesis and no words are adequate to express my appreciation to both of them.

Dedication

This thesis is dedicated to my mother, my father, my wife and my child.

Table of contents

Author's declaration.....	ii
Acknowledgement.....	iii
Dedication	v
Table of contents	vi
List of Figures	xii
List of symbols.....	xx
List of abbreviations.....	xxi
ABSTRAK	xxii
ABSTRACT	xxiv
CHAPTER 1	1
INTRODUCTION	1
1.1 Research background	1
1.2 Problem statement	4
1.3 Research objectives	6
1.4 Project approach	6
CHAPTER 2	8
LITERATURE REVIEW.....	8
2.1 Ceramic cutting insert	8
2.2 Al ₂ O ₃ as a cutting insert	9
2.3 Disadvantages of Al ₂ O ₃ as a cutting insert.....	9
2.4 Yttria stabilized zirconia (YSZ)	10
2.5 Zirconia toughened Al ₂ O ₃ (ZTA).....	11
2.6 Fabrication method.....	13
2.6.1 Sintering	14
2.7 Effect of additives	16
2.7.1 Effect of MgO addition to Al ₂ O ₃	16
2.7.2 Effect of Cr ₂ O ₃ addition to Al ₂ O ₃	19
2.8 Effect of particle size and grain size on mechanical properties	23
2.9 Effect of mechanical properties on tool wear.....	24
2.10 Characterizations	29

2.10.1	Tool wear.....	29
2.10.2	Vickers hardness and fracture toughness	31
2.10.3	Microstructural observation	38
2.10.4	Effect of microstructure on mechanical properties	42
2.10.5	Bulk density and shrinkage	43
2.10.6	X-ray diffraction.....	47
2.11	Summary	51
CHAPTER 3		52
MATERIALS AND METHODOLOGY		52
3.1	Experimental Design	52
3.2	Part 1: Effect of MgO addition on mechanical properties, microstructure and tool wear of ZTA cutting insert	56
3.2.1	Calculations.....	56
3.2.2	Mixing.....	57
3.2.3	Compaction	57
3.2.4	Sintering	58
3.2.6	Shrinkage analysis.....	59
3.2.7	Bulk density and porosity measurement	59
3.2.8	Vickers hardness and fracture toughness	60
3.2.9	Microstructural observation	61
3.2.10	Machining	62
3.2.11	Tool wear measurement	63
3.3	Part 2: Effect of MgO particle size on the mechanical properties, microstructure and tool wear of ZTA cutting insert	64
3.3.1	Calculations.....	64
3.3.2	Mixing.....	64
3.3.3	Compaction	65
3.3.4	Sintering	65
3.3.5	Characterization method	65
3.4	Part 3: Effect of Cr ₂ O ₃ addition on the mechanical properties, microstructure and tool wear of ZTA and ZTA-MgO ceramic composite	66
3.4.1	Calculations.....	66
3.4.2	Sample preparation.....	67
3.4.3	Characterization method	67

CHAPTER 4	68
RESULT AND DISCUSSION	68
4.1 Introduction	68
4.2 Characterization of starting materials.....	68
4.2.1 Al ₂ O ₃	68
4.2.2 YSZ	70
4.2.3 MgO	73
4.2.4 Cr ₂ O ₃	74
4.3 Part 1: Results and discussions on the effect of MgO addition on the mechanical properties, microstructures and tool wear of ZTA cutting insert.	76
4.3.1 XRD	76
4.3.2 Microstructural observation, shrinkage analysis, bulk density, percentage of porosity, Vickers hardness and fracture toughness.	80
4.2.3 Tool wear measurement	91
4.2.4 Summary	97
4.4 Part 2: Results and discussions on the effect of MgO particle sizes on the mechanical properties, microstructures and tool wear of ZTA cutting insert.	97
4.4.1 XRD	97
4.4.2 Microstructural observation, shrinkage analysis, bulk density, percentage of porosity, Vickers hardness and fracture toughness.	102
4.4.3 Tool wear measurement	116
4.4.4 Summary	122
4.5 Part 3: Results and discussions on the effect of Cr ₂ O ₃ addition on the mechanical properties, microstructures and tool wear of ZTA and ZTA-20 nm MgO cutting insert.....	123
4.5.1 Introduction.....	123
4.5.2 Macro observation.....	123
4.5.3 XRD	124
4.5.4 Microstructural observation, shrinkage analysis, bulk density, percentage of porosity, Vickers hardness and fracture toughness.	130
4.5.5 Tool wear measurement	143
4.5.6 Summary	151
CHAPTER 5	153
CONCLUSION AND FUTURE RECOMMENDATION	153
5.1 Conclusion.....	153

5.2	Future recommendations	154
REFERENCES.....		156
APPENDICES		

List of Tables

Table 2.1: Mechanical properties of Al_2O_3 (Al-Naib, 2000).	9
Table 2.2: Summary of mechanical properties of Al_2O_3 contain different amount of Cr_2O_3 (Riu <i>et al.</i> , 2000).	21
Table 2.3: Properties of Al_2O_3 - Ag_2O composites (Dutta <i>et al.</i> , 2006).....	26
Table 2.4: Properties of the studied dense ceramics (Medvedovski, 2001).....	27
Table 2.5: Summarize result for V_B max for various ceramics inserts (D'Errico <i>et al.</i> , 1999).	29
Table 2.6: Vickers Hardness for ceramic cutting inserts (D' Errico <i>et al.</i> , 1999)	32
Table 2.7: Sintering profiles used by Smuk <i>et al.</i> (2003) for mechanical characterizations (Smuk <i>et al.</i> , 2003).....	33
Table 2.8: Compositions used by Smuk <i>et al.</i> (2003) for mechanical charactrerization (Smuk <i>et al.</i> , 2003).....	34
Table 2.9: Vickers hardness and fracture toughness of the sintered samples (Magnani and Brilliante, 2005).....	37
Table 2.10: Results of grain size for YSZ- Al_2O_3 at different compositions (Cesari <i>et al.</i> , 2006).....	39
Table 2.11: Al_2O_3 grain sizes for Al_2O_3 -MgO system with 4.0 wt % Cr_2O_3 addition (Sarkar <i>et al.</i> , 2002).....	41
Table 2.12: Grain size, relative density, Vickers hardness and fracture toughness of pure Al_2O_3 samples sintered at 1500 °C (Maiti and Sil, 2010).....	44
Table 2.13: Densities and shrinkage of the Al_2O_3 -MgO ceramics with different MgO contents (Rittidech <i>et al.</i> , 2006).....	45
Table 2.14: Unit cell parameter for a and c for Al_2O_3 with the addition of Cr_2O_3 (Bondioli <i>et al.</i> , 2000).....	49
Table 3.1: Raw materials used in current study.	52
Table 3.2: Formulations used in Part 1.....	57
Table 3.3: Cutting parameter for using ceramic cutting insert.....	62

Table 3.4: Physical and mechanical properties of the workpiece, stainless steel 316L.....	62
Table 3.5: Formulations used in Part 2.....	65
Table 3.6: Formulations used for ZTA samples.....	67
Table 3.7: Formulations used for ZTA-MgO samples	67
Table 4.1: Elemental quantitative analysis on the YSZ particles.....	72
Table 4.2: Particle sizes for MgO used in current study.	73
Table 4.3: Shrinkage result for ZTA sample with different wt % and different particle sizes of MgO.	109
Table 4.4: Unit cell dimensions of Al ₂ O ₃ with different Cr ₂ O ₃ wt %.	126

List of Figures

Fig. 1.1:	Relationship between cutting speed and tool life for typical materials for cutting insert application (Kalpakjian and Schmid, 2009).	2
Fig. 1.2:	Relationship between temperature and hardness for typical materials for cutting insert (Kalpakjian and Schmid, 2009).	3
Fig. 2.1:	Grain structure of zirconium oxide (light grey) in aluminium oxide (dark-grey). The horizontal bar has a length of 1 micron (Casellas <i>et al.</i> , 1999).	12
Fig. 2.2:	Micrograph for (a) monolithic Al ₂ O ₃ and (b) 80 wt % Al ₂ O ₃ /20 % YSZ (Azhar <i>et al.</i> , 2009).	13
Fig. 2.3:	Stages of sintering (a) free particles, (b) necking between particles, (c) formation of grain boundary, and (d) densification process and pores elimination (Randal, 1991).	15
Fig. 2.4:	Densification of Al ₂ O ₃ compacts with and without MgO additives. TSI stands for tons per square inch (Coble, 1961).	16
Fig. 2.5:	Grain growth in Al ₂ O ₃ compacts with temperature, forming pressure and magnesia additives as variables (Coble, 1961).	17
Fig. 2.6:	Phase diagram of the system MgO–Al ₂ O ₃ (Sarkar and Banerjee, 1999).	18
Fig. 2.7:	Morphologies of Al ₂ O ₃ specimens hot pressed at 1500°C for 1 h containing (A) 0 mol%, (B) 2 mol%, (C) 5 mol%, and (D) 10 mol% of Cr ₂ O ₃ (Riu <i>et al.</i> , 2000).	20
Fig. 2.8:	Morphology of platelike grains, shown by the arrow in the figure (Riu <i>et al.</i> , 2000).	21
Fig. 2.9:	Phase relationship between Al ₂ O ₃ -Cr ₂ O ₃ (Hirata <i>et al.</i> , 2000).	22
Fig. 2.10:	Flank wear with machining time (Dutta <i>et al.</i> , 2006).	26
Fig. 2.11:	Wear pattern observed during turning process for ceramic cutting insert (a) primary edge breakage, (b) chipping, (c) edge breakage, (d) notch wear, © chip hammering and (f) flank wear (Cantero <i>et al.</i> , 2013).	28
Fig. 2.12:	Schematics of the insert wear measurement system (Shahabi and Ratnam, 2008)	30

Fig. 2.13: (a) Unworn cutting insert tip, (b) worn cutting insert tip after machining, and (c) tool wear (Shahabi and Ratnam, 2008).	31
Fig. 2.14: Vickers hardness of the Al_2O_3 –MgO ceramics with variation of MgO contents (Rittidech <i>et al.</i> , 2006).	32
Fig. 2.15: Result for Vickers hardness under different sintering temperature and different compositions (Smuk <i>et al.</i> , 2003).	33
Fig. 2.16: Vickers hardness of Al_2O_3 -5 vol % SiC nanocomposite as a function of MgO content when sintered at 1650 °C for 2 hours in argon atmosphere (Wang <i>et al.</i> , 1998).	34
Fig. 2.17: Result for fracture toughness under different sintering temperature and different compositions (Smuk <i>et al.</i> , 2003).	36
Fig. 2.18: Configurations of the Palmqvist cracks for the Vickers hardness indentation, a is half of the indent diagonal and l is length of the crack (Smuk <i>et al.</i> , 2003).	38
Fig. 2.19: Microstructure of: (a) Al_2O_3 ceramics with 30 mass% of stabilized ZrO_2 (b) standard Al_2O_3 ceramics SN80 (Smuk <i>et al.</i> , 2003).	39
Fig. 2.20: SEM micrographs showing microstructural evolution in ZTA (a) as-sintered, and (b) heat treated at 1600 °C for 30 h (Casellas <i>et al.</i> , 2003).	40
Fig. 2.21: SEM micrographs of as-received of Al_2O_3 –MgO ceramics with different MgO contents at (a) 0 wt.%, (b) 0.05 wt.% (c) 0.10 wt.%, (d) 0.30 wt.%, © 0.50 wt.%, and (f) 0.70 wt.%, respectively (Rittidech <i>et al.</i> , 2006).	41
Fig. 2.22: Micrograph of Al_2O_3 -MgO system with 4.0 wt % Cr_2O_3 addition, (a) 71.67 wt % Al_2O_3 , 28.33 wt % MgO, (b) 55.78 wt % Al_2O_3 , 44.22 wt % MgO, and (c) 83.49 wt % Al_2O_3 , 16.51 wt % MgO (Sarkar <i>et al.</i> , 2002).	42
Fig. 2.23: EDX analysis on ZTA sample sintered at 1700 °C (a) Al_2O_3 –5 wt% ZrO_2 and (b) Al_2O_3 –5 wt% ZrO_2 –1000 ppm $\text{Y}(\text{NO}_3)_3 \cdot 6\text{H}_2\text{O}$ (Maiti and Sil, 2011).	43
Fig. 2.24: SEM micrograph of Al_2O_3 sintered at 1500 °C for (a) 3 h, (b) 6 h, (c) 18 h and (d) 24 h (Maiti and Sil, 2010).	44
Fig. 2.25: Sintered density of Al_2O_3 -5 vol % SiC nanocomposite as a function of MgO content when sintered at 1650 °C for 2 hours in argon atmosphere (Wang <i>et al.</i> , 1998).	46

Fig. 2.26: Relationship between relative densities of $\text{Al}_2\text{O}_3\text{-Cr}_2\text{O}_3$ with sintering temperature (Hirata <i>et al.</i> , 2000).	46
Fig. 2.27: Result of percentage of shrinkage with Cr_2O_3 addition for (a) 71.67 wt % Al_2O_3 , 28.33 wt % MgO, (b) 55.78 wt % Al_2O_3 , 44.22 wt % MgO, and (c) 83.49 wt % Al_2O_3 , 16.51 wt % MgO (Sarkar <i>et al.</i> , 2002).	47
Fig. 2.28: XRD for (a) ZrO_2 , and (b) YSZ (Smuk <i>et al.</i> , 2003).	48
Fig. 2.29: XRD patterns of (012) peak of solid solutions with (a)10, (b) 30, (c) 50, (d) 90 wt% of chromium oxide, (E) eskolaite, and (C) corundum (Bondioli <i>et al.</i> , 2000).	49
Fig. 2.30: Comparison of XRD pattern for MgO-2 wt % nano and micro- Cr_2O_3 samples sintered at 1450 °C for 5 hours (Zargar <i>et al.</i> , 2012).	50
Fig. 2.31: XRD scans of Ti/Ti-B composite with different reinforcement composite particle sizes (Patel <i>et al.</i> , 2009).	51
Fig. 3.1: Flowchart for Part 1 (To study the effect of MgO additives on the mechanical properties of ZTA ceramic composite).	53
Fig. 3.2: Flowchart for Part 2 (To study the effect of MgO particles sizes on the mechanical properties of ZTA ceramic composite).	54
Fig. 3.3: Flowchart for Part 3 (To study the effect of Cr_2O_3 additives on the mechanical properties of ZTA and ZTA-MgO ceramic composite).	55
Fig. 3.4: Dimension of the die used to produce samples for tool wear measurement. All value is in mm.	58
Fig. 3.5: Sintering profile used to sinter the green body.	58
Fig. 3.6: Indentation schematic for Vickers hardness test.	60
Fig. 3.7: Typical crack configuration for determination of fracture toughness a is half of the indent length and c stand for the crack length.	61
Fig. 3.8: Heating profile used for thermal etching.	62
Fig. 3.9: The flowchart of steps in order to obtain results of tool wear.	63
Fig. 3.10: Print screen of the software used to subtract image of cutting insert before and after machining and calculate tool wear.	64

Fig. 4.1:	Result of particles size analysis for Al_2O_3 particles.....	69
Fig. 4.2:	Physical appearance of Al_2O_3 particles (a) magnification 5000 X, (b) magnification 20 000 X.	69
Fig. 4.3:	XRD result for Al_2O_3 particles, ICDD reference 10-0173.....	70
Fig. 4.4:	Results of particle size for YSZ particles.....	70
Fig. 4.5:	Physical appearance of YSZ particles (a) magnification 5000 X, (b) magnification 20 000 X.	71
Fig. 4.6:	EDX characterizations of YSZ particles.	72
Fig. 4.7:	XRD results for YSZ powders, ICDD reference file for tetragonal (red lines) and monoclinic (blue lines) are 89-9068 and 78-1807 respectively.	72
Fig. 4.8:	Results for particles size for nano-MgO.	73
Fig. 4.9:	XRD results for MgO nano particles, which (s) is MgO with ICDD reference 98-005-3326 and (o) is brucite with ICDD reference 98-004-4736.	74
Fig. 4.10:	XRD diffractions for MgO with different particle sizes.....	75
Fig. 4.11:	Results of particle size for Cr_2O_3	75
Fig. 4.12:	XRD results for Cr_2O_3 powder, ICDD reference 01-082-1484.....	75
Fig. 4.13:	Morphology of Cr_2O_3 particles.	76
Fig. 4.14:	XRD result for ZTA+ 0.7 MgO wt % after sintering process.....	77
Fig. 4.15:	XRD diffraction for ZTA with 0 wt % MgO for (a) before sintering, and (b) after sintering.	78
Fig. 4.16:	Result of XRD analysis on ZTA–MgO sintered body with different MgO wt%. Peak shown is for (111), MgAl_2O_4 (ICDD 01-073-1959).....	79
Fig. 4.17:	Quantitative elemental analysis on the sample for (a) YSZ and (b) Al_2O_3	81
Fig. 4.18:	Microstructural images of the samples surface (a) 0 wt% MgO, (b) 0.3 wt% MgO, (c) 0.5 wt% MgO, (d) 0.7 wt% MgO, (e) 0.9 wt% MgO, and (f) 1.0 wt% MgO.....	82

Fig. 4.19: N_L values for Al_2O_3 grains with different MgO wt %.	83
Fig. 4.20: Result of shrinkage of ZTA with different MgO wt %.	84
Fig. 4.21: Result of density and percentage of porosity for ZTA with different MgO wt %.	86
Fig. 4.22: Result of Vickers hardness for ZTA as a function of MgO wt %.	88
Fig. 4.23: Result of fracture toughness as a function of MgO wt%.	89
Fig. 4.24: Images of cutting inserts (a) unworn, (b) example of a worn cutting insert (c) 0 wt %, (d) 0.1 wt %, (e) 0.2 wt %, and (f) 0.5 wt %.	92
Fig. 4.25: Result of tool wear for ZTA cutting insert at various addition of MgO wt %.	93
Fig. 4.26: Result of flank wear for ZTA cutting insert at various addition of MgO wt %.	93
Fig. 4.27: Relationship between bulk density and tool wear for ZTA-MgO cutting insert.	94
Fig. 4.28: Relationship between Vickers hardness and tool wear for ZTA-MgO cutting insert.	95
Fig. 4.29: Relationship between fracture toughness and tool wear for ZTA-MgO cutting insert.	96
Fig. 4.30: Result of XRD analysis on ZTA–20 nm MgO sintered body with different MgO wt%. Peak shown is for (111), $MgAl_2O_4$ (ICDD 01-073-1959).	99
Fig. 4.31: Result of XRD analysis on ZTA–500 nm MgO sintered body with different MgO wt%. Peak shown is for (111), $MgAl_2O_4$ (ICDD 01-073-1959).	100
Fig. 4.32: Result of XRD analysis on ZTA–7000 nm MgO sintered body with different MgO wt%. Peak shown is for (111), $MgAl_2O_4$ (ICDD 01-073-1959).	101
Fig. 4.33: FESEM microstructural images for ZTA- 0.9 MgO wt % ; (a) 20 nm MgO ($N_L = 2.54$ grain/ μm), (b) 100 nm MgO ($N_L = 2.21$ grain/ μm), (c) 500 nm MgO ($N_L = 1.27$ grain/ μm) and (d) 7000 nm ($N_L = 0.51$ grain/ μm).	103

Fig. 4.34: N_L values for Al_2O_3 grain for ZTA with different particle sizes of MgO.	104
Fig. 4.35: FESEM microstructural images for ZTA- 20 nm MgO as additives (a) 0.3 wt % MgO, (b) 0.5 wt % MgO, (c) 0.7 wt % MgO, (d) 0.9 wt % MgO, (e) 1.1 wt % MgO and (f) 1.3 wt % MgO. All micrograph is taken with 5000 X magnification.	105
Fig. 4.36: FESEM microstructural images for ZTA-100 nm MgO as additives (a) 0.3 wt % MgO, (b) 0.5 wt % MgO, (c) 0.6 wt % MgO, (d) 0.7 wt % MgO, (e) 0.8 wt % MgO and (f) 0.9 wt % MgO. All micrograph is taken with 5000 X magnification.	106
Fig. 4.37: FESEM microstructural images for ZTA-500 nm MgO as additives (a) 0.3 wt % MgO, (b) 0.5 wt % MgO, (c) 0.6 wt % MgO, (d) 0.7 wt % MgO, (e) 0.8 wt % MgO and (f) 0.9 wt % MgO. All micrograph is taken with 5000 X magnification.	107
Fig. 4.38: FESEM microstructural images for ZTA-7000 nm MgO as additives (a) 0.3 wt % MgO, (b) 0.5 wt % MgO, (c) 0.7 wt % MgO, (d) 0.5 wt % MgO and (e) 0.8 wt % MgO and (f) 0.9 wt % MgO. All micrograph is taken with 5000 X magnification.	108
Fig. 4.39: Result of bulk densities as a function of MgO wt % with different particles sizes.	110
Fig. 4.40: Percentage of porosity for ZTA samples with different particle sizes and composition.	112
Fig. 4.41: Result of Vickers hardness as a function of MgO wt % with different particle sizes.	114
Fig. 4.42: Result of fracture toughness as a function of MgO wt % with different particle sizes.	116
Fig. 4.43: Images of ZTA-MgO cutting inserts different particle sizes (a) before machining, (b) after machining, (c) 20 nm, (d) 100 nm, (e) 500 nm, and (f) 7000 nm.	117
Fig. 4.44: Tool wear after machining stainless steel 316L for cutting insert with different particle sizes. Amount of MgO was fixed at 0.3 wt %	119
Fig. 4.45: Flank wear after machining stainless steel 316L for cutting insert with different particle sizes. Amount of MgO was fixed at 0.3 wt %	119

Fig. 4.46: Relationship between bulk density and tool wear for ZTA-MgO cutting insert with different particles sizes. Amount of MgO was fixed to 0.3 wt %.	120
Fig. 4.47: Relationship between Vickers hardness and tool wear for ZTA-MgO cutting insert with different particles sizes. Amount of MgO was fixed to 0.3 wt %.	121
Fig. 4.48: Relationship between fracture toughness and tool wear for ZTA-MgO cutting insert with different particles sizes. Amount of MgO was fixed to 0.3 wt %.	122
Fig. 4.49: Sintered samples of (a) ZTA-0.6 wt % Cr ₂ O ₃ , and (b) ZTA-20 nm MgO-0.6 wt % Cr ₂ O ₃ .	123
Fig. 4.50: XRD analysis for ZTA-0.6 wt % Cr ₂ O ₃ .	125
Fig. 4.51: XRD patterns of (012) peak of pure Al ₂ O ₃ , ZTA with different Cr ₂ O ₃ content and pure Cr ₂ O ₃ .	126
Fig. 4.52: Comparison of XRD results for ZTA samples with various Cr ₂ O ₃ wt %.	127
Fig. 4.53: XRD results of addition of 1.0 % Cr ₂ O ₃ into ZTA-20 nm MgO cutting insert.	128
Fig. 4.54: Comparison of XRD results for ZTA-MgO samples with various Cr ₂ O ₃ wt %.	129
Fig. 4.55: Microstructural images of ZTA-Cr ₂ O ₃ cutting inserts with addition of (a) 0 wt% Cr ₂ O ₃ , (b) 0.2 wt% Cr ₂ O ₃ , (c) 0.3 wt% Cr ₂ O ₃ , (d) 0.5 wt% of Cr ₂ O ₃ , (e) 0.6 wt% of Cr ₂ O ₃ (arrow indicated platelike grain) and (f) 0.7 wt% of Cr ₂ O ₃ . All micrograph were taken with 5000 X magnification.	131
Fig. 4.56: Number of Al ₂ O ₃ grain interception per unit length for ZTA samples with different Cr ₂ O ₃ wt %.	132
Fig. 4.57: EDX results for ZTA-samples which containing 0.8wt% Cr ₂ O ₃ .	133
Fig. 4.58: Microstructural images of ZTA-MgO-Cr ₂ O ₃ samples with addition of (a) 0.4 wt% Cr ₂ O ₃ , (b) 0.6 wt% Cr ₂ O ₃ , and (c) 0.8 wt% Cr ₂ O ₃ .	134
Fig. 4.59: Number of Al ₂ O ₃ grain interception per unit length for ZTA-MgO samples with different Cr ₂ O ₃ wt %.	135

Fig. 4.60: EDX results for ZTA-20 nm MgO samples which containing 0.4wt% of Cr ₂ O ₃	136
Fig. 4.61: Result of shrinkage of ZTA and ZTA-MgO samples with various Cr ₂ O ₃ wt % after sintering.....	137
Fig. 4.62: Result of bulk density for ZTA–Cr ₂ O ₃ and ZTA- Cr ₂ O ₃ -20nm MgO cutting inserts with different Cr ₂ O ₃ content.....	138
Fig. 4.63: Percentage of porosity for ZTA–Cr ₂ O ₃ and ZTA- Cr ₂ O ₃ -20nm MgO cutting inserts with different Cr ₂ O ₃ content.....	139
Fig. 4.64: Vickers hardness of ZTA and ZTA-20 nm MgO samples as a function of Cr ₂ O ₃ wt%.....	141
Fig. 4.65: Fracture toughness of ZTA and ZTA-20 nm MgO samples as a function of Cr ₂ O ₃ wt%.....	142
Fig. 4.66: Images of cutting inserts (a) unworn, (b) example of a worn cutting insert, (c) ZTA-20 nm MgO-0.6 Cr ₂ O ₃ wt%, and (d) ZTA-0.6 Cr ₂ O ₃ wt%.	144
Fig. 4.67: Result of tool wear for ZTA and ZTA-10 nm MgO cutting insert with different Cr ₂ O ₃ wt %.	145
Fig. 4.68: Flank wear measurement for ZTA and ZTA-20 nm MgO cutting insert with the addition of 0.6 wt % of Cr ₂ O ₃	145
Fig. 4.69: Tool wear of ZTA-20 nm MgO-Cr ₂ O ₃ cutting insert at different machining speed.....	148
Fig. 4.70: Relationship between bulk density and tool wear for ZTA and ZTA-20 nm MgO cutting insert.	149
Fig. 4.71: Relationship between Vickers hardness and tool wear for ZTA and ZTA-20 nm MgO cutting insert.	151
Fig. 4.72: Relationship between fracture toughness and tool wear for ZTA and ZTA-20 nm MgO cutting insert.	151

List of symbols

a	- Half of the indentation diagonal length
a	- Lattice parameter a
c	- Lattice parameter c
d_{50}	- Mean diameter
E	- Modulus Young
HV	- Vickers hardness
K_{Ic}	- Fracture toughness
l	- Length of the radiant crack
l_i	- Initial length of sample
l_f	- Final length of sample
(t)	- Tetragonal phase
(m)	- Monoclinic phase
ρ_b	- Bulk density
N_L	- Number of grains intercept per unit length

List of abbreviations

ASTM	- American Standard for Testing Materials
BUE	- Build up edge
EDX	- Energy Dispersive X-ray
FESEM	- Field Emission Scanning Electron Microscope
ICDD	- International Centre for Diffraction Data
ISO	- International Standard Organization
MPa	- Mega Pascal
MOR	- Modulus of rupture
HV	- Vickers hardness
SEM	- Scanning Microscope Electron
TSI	- Tonne per square inch
TEM	- Transmission Electron Microscope
XRD	- X-ray diffraction
YSZ	- Yttria stabilized zirconia
ZTA	- Zirconia toughened alumina

SINTESIS DAN PENCIRIAN BAHAN ALAT PEMOTONG MgO-Cr₂O₃-ZTA

ABSTRAK

Dalam kajian ini, kesan penambahan MgO dan Cr₂O₃ terhadap mikrostruktur dan ciri-ciri mekanikal komposit seramik ZTA telah dikaji. Pelbagai amaun MgO dan Cr₂O₃ ditambah ke dalam ZTA secara berasingan. Bahan mula dicampur berterusan selama 8 jam dan kemudiannya dipadatkan secara hidraulik pada 300 MPa. Sampel-sampel yang telah dipadatkan di sinter pada 1600 °C selama 4 jam. Terdapat tiga bahagian dalam kajian ini. Bahagian pertama terdiri dari penambahan MgO ke dalam ZTA. Bahagian kedua difokuskan kepada kesan saiz partikel MgO terhadap sifat-sifat mekanikal dan bahagian ketiga difokuskan terhadap kesan penambahan Cr₂O₃ terhadap sistem ZTA and ZTA-20 nm MgO. Untuk bahagian pertama, keputusan menunjukkan penambahan 0.7 wt % MgO bersaiz 100nm menghasilkan kekerasan Vickers tertinggi (1710HV). Keliatan patah berkurang secara berterusan dari 5.93 MPa.m^{1/2} kepada 3.79 MPa.m^{1/2} dengan penambahan sebanyak 1.0 MgO wt %. Keterlarutan pepejal MgO di dalam ZTA dianggarkan sebanyak 203 ppm. Tiada mekanisme baru yang ditemui dengan penambahan MgO ke dalam ZTA. Pemerhatian terhadap mikrostruktur menunjukkan nilai N_L untuk saiz butir sangat bergantung kepada amaun MgO yang ditambah. Nilai N_L meningkat dari 0.68 butir/μm to 2.21 butir/μm dengan penambahan 0.7 wt % MgO. Peningkatan kekerasan Vickers disebabkan oleh kesan pin mikrostruktur oleh MgO. Dalam pengukuran kehausan mata alat, peningkatan sebanyak 30 % ditunjukkan oleh sampel ZTA dengan 0.3 MgO wt %. Untuk bahagian kedua, saiz partikel MgO dipelbagai dari 20 nm hingga 7000 nm. Pemerhatian menunjukkan MgO dengan saiz yang lebih halus akan meningkatkan kecekapan kesan pin; satu kelebihan yang ditunjukkan oleh MgO. Sampel ZTA dengan bahan tambah 20 nm MgO mempunyai saiz butir Al₂O₃ yang halus (2.50 grains/μm) berbanding dengan ZTA dengan 100 nm MgO (2.21 grains/μm), 500 nm MgO (1.27 grains/μm) dan 7000 nm MgO (0.81 grains/μm). Saiz butir ZTA dengan 20 nm MgO yang halus menyebabkan kekerasan Vickers yang tinggi (1740HV) tetapi keliatan patah 3.62 MPa.m^{1/2}. Pembentukan MgAl₂O₄ dikesan pada pelbagai komposisi MgO untuk setiap saiz partikel, dimana 1.1 wt % untuk 20 nm MgO, 0.7 wt % untuk 100 nm MgO, 0.6 wt % untuk 500 nm MgO untuk 0.5 wt % for 7000 nm MgO. Pengukuran mata alat menunjukkan sampel ZTA dengan 20 nm MgO menunjukkan peningkatan sebanyak 54.8 % berbanding

sampel ZTA dengan 100 nm MgO. Untuk bahagian ketiga, amaun Cr_2O_3 dari 0 wt % - 1.0 wt % diperkenalkan kepada dua sistem berbeza; ZTA dan ZTA dengan 20 nm 1.1 wt % MgO. Sampel ZTA dengan penambahan 0.6 wt % menghasilkan kekerasan Vickers setinggi 1683 HV dan keliatan patah $7.05 \text{ MPa.m}^{1/2}$. Peningkatan kekerasan Vickers disebabkan oleh penambahan Cr_2O_3 , yang mana mempunyai kekerasan yang lebih tinggi dari ZTA. Peningkatan keliatan patah disebabkan oleh saiz butir Al_2O_3 yang besar dan kehilangan fasa monoklinik di dalam YSZ. Berdasarkan kepada analisis XRD, tiada pembentukan fasa baru terhasil dengan penambahan Cr_2O_3 memandangkan kedua-dua Cr_2O_3 dan Al_2O_3 adalah dalam keterlarutan pepejal sepenuhnya. Nilai N_L untuk sampel ZTA berkurangan dengan penambahan 0.6 wt % Cr_2O_3 dari 1.30 butir/ μm kepada 0.78 butir/ μm . Sampel ZTA-20 nm MgO- Cr_2O_3 mempunyai kekerasan Vickers yang lebih tinggi (1693HV) dan kehausan mata alat yang lebih rendah (0.015 mm^2) berbanding kepada ZTA- Cr_2O_3 (1683 HV and 0.0190 mm^2). Keputusan pengukuran kehausan mata alat menunjukkan sampel ZTA-20nm MgO- Cr_2O_3 mempunyai peningkatan sebanyak 25 % berbanding sampel ZTA- Cr_2O_3 . Keseluruhannya, sampel ZTA-1.1 wt % 20 nm MgO-0.6 wt % Cr_2O_3 adalah komposisi terbaik untuk aplikasi mata alat.

SYNTHESIS AND CHARACTERIZATION OF MgO-Cr₂O₃-ZTA CUTTING TOOL MATERIAL

ABSTRACT

The effect of MgO and Cr₂O₃ addition on the microstructure and mechanical properties of ZTA ceramic composite were investigated in this study. Various amounts of MgO and Cr₂O₃ were added into ZTA separately. The starting materials was mixed continuously for 8 hours and subsequently hydraulically pressed at 300 MPa. The pressed samples were sintered at 1600 °C for 4 hours. There are three parts in this study. The first part consists of addition of MgO into ZTA. Second part is focused on the effect of MgO particles sizes on ZTA mechanical properties and the third part is focused on the effect of adding Cr₂O₃ on ZTA and ZTA-20 nm MgO. For the first part, the results show that an addition of 0.7 wt % of 100 nm MgO produces the highest Vickers hardness (1710 HV). The fracture toughness decreased gradually from 5.93 MPa.m^{1/2} to 3.79 MPa.m^{1/2} with further addition of 1.0 MgO wt %. MgO solid solubility in ZTA was determined around 203 ppm. No new mechanism was found with the addition of MgO into ZTA. Microstructural observations show that the N_L value for grain size is significantly dependent on the amount of MgO addition. The N_L value increase from 0.68 grains/μm to 2.21 grains/μm with the addition of 0.7 wt % of 100 nm MgO. The increase of hardness is due to the small grain size of Al₂O₃ which is caused by the microstructure pinning effect by MgO. In tool wear measurement, an improvement of 30 % is shown for ZTA sample with 0.3 MgO wt %. For the second part, the particle sizes of MgO were varied from 20 nm to 7000 nm. It was observed that finer size of MgO enhances the microstructure pinning effect; a feature introduce by MgO. ZTA samples with additives of 20 nm of MgO were found to have fine Al₂O₃ grain size (2.50 grains/μm) compared to ZTA with 100 nm MgO (2.21 grains/μm), 500 nm MgO (1.27 grains/μm) and 7000 nm MgO (0.81 grains/μm). The fine grain of ZTA with 20 nm MgO leads to a high Vickers hardness (1740 HV) but a fracture toughness of 3.62 MPa.m^{1/2}. Formation of MgAl₂O₄ was detected at different composition of each MgO particle sizes, whereas 1.1 wt % for 20 nm MgO, 0.7 wt % for 100 nm MgO, 0.6 wt % for 500 nm MgO and 0.5 wt % for 7000 nm MgO. Tool wear measurement indicated that ZTA samples with 20 nm MgO shows an increase of 54.8 % compare to ZTA samples with 100 nm MgO. For the third part of the study, amounts from 0

wt % - 1.0 wt % of Cr_2O_3 are introduced into two separate systems: ZTA and ZTA with 20 nm 1.1 wt % MgO. ZTA samples with the addition of 0.6 wt % of Cr_2O_3 produced Vickers hardness of 1683HV and fracture toughness of $7.05 \text{ MPa}\cdot\text{m}^{1/2}$. The increase of Vickers hardness is attributed to the addition of Cr_2O_3 , which has higher hardness than ZTA. The increase of fracture toughness is due to the large Al_2O_3 grain and the loss of monoclinic phase inside YSZ due to the presence of Cr_2O_3 . According to XRD analysis, no new phase was formed with the addition of Cr_2O_3 since both Cr_2O_3 and Al_2O_3 are in complete solid solubility with each other. N_L values for ZTA samples decrease with the addition of 0.6 wt % Cr_2O_3 from 1.30 grains/ μm to 0.78 grains/ μm . Sample of ZTA-20 nm MgO- Cr_2O_3 has higher Vickers hardness (1693HV) and lower tool wear (0.015 mm^2) compared to ZTA- Cr_2O_3 (1683 HV and 0.0190 mm^2). Result of tool wear measurement shows that sample of ZTA-20 nm MgO- Cr_2O_3 has 35 % of improvement compare to ZTA- Cr_2O_3 . In overall, samples of ZTA-1.1 wt % 20 nm MgO-0.6 wt % Cr_2O_3 is the best composition for cutting insert application.

CHAPTER 1

INTRODUCTION

1.1 Research background

Products produce by processes such as casting and forming regularly need additional process or finishing imparting a detailed characteristic for instance dimensional accuracy and surface finish. Turning process is one of the alternatives used to accomplish surface finish and removal of materials.

Extremely hard materials can be machined using cutting insert with high heat and wear resistant. Furthermore, these cutting insert are also chemically stable at high temperature. The mentioned features enabled them to machine hard metals at high cutting speed in dry environment. Another advantage of ceramic cutting insert is that the tips of these cutting insert does not require cooling liquid to reduce the operating temperature. New cutting insert with improved performance and properties are produced with the advancement in the technology of ceramic processing. These new developed cutting inserts has enabled ceramic cutting insert to machine various types of metals (Senthil Kumar *et al.*, 2003).

Furthermore, cutting insert with high quality and prolonged life can reduce the cost for machining. Based on the requirement of prolonged life and high-quality cutting inserts, cutting inserts made from metal oxides or ceramics offers a wide selection of materials such as Sialon, Si_3N_4 , Al_2O_3 -based, cemented carbide and zirconia toughened Al_2O_3 (ZTA) cutting inserts.

Fig. 1.1 shows the relationship between cutting speed and tool life for typical materials for cutting insert applications. Cutting inserts made from ceramic are able to perform at higher cutting speed and possess longer tool life compare to other types of materials (Kalpakjian and Schmid, 2009).

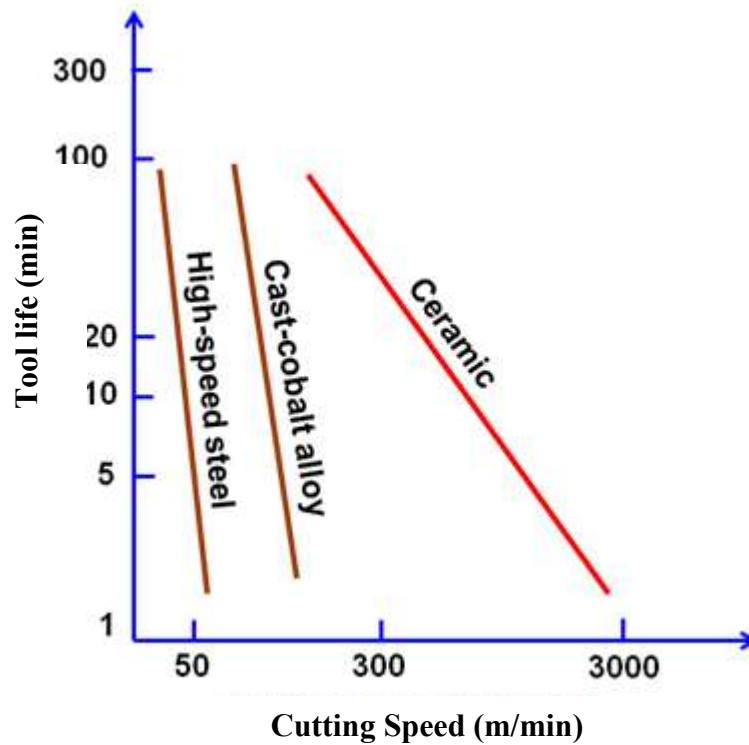


Fig. 1.1: Relationship between cutting speed and tool life for typical materials for cutting insert application (Kalpakjian and Schmid, 2009).

Besides longer tool life, another advantage of ceramic cutting inserts is their ability to retain high hardness at higher temperature. During machining process, the friction between the cutting insert and the workpiece will generate heat. Generating too much heat will reduce the mechanical properties of the cutting insert thus decreasing the tool life. Fig. 1.2 shows the relationship between temperature and hardness for typical materials for cutting insert materials. Cutting insert made from ceramics shows small reduction of hardness with increasing temperature, compared to other types of cutting insert.

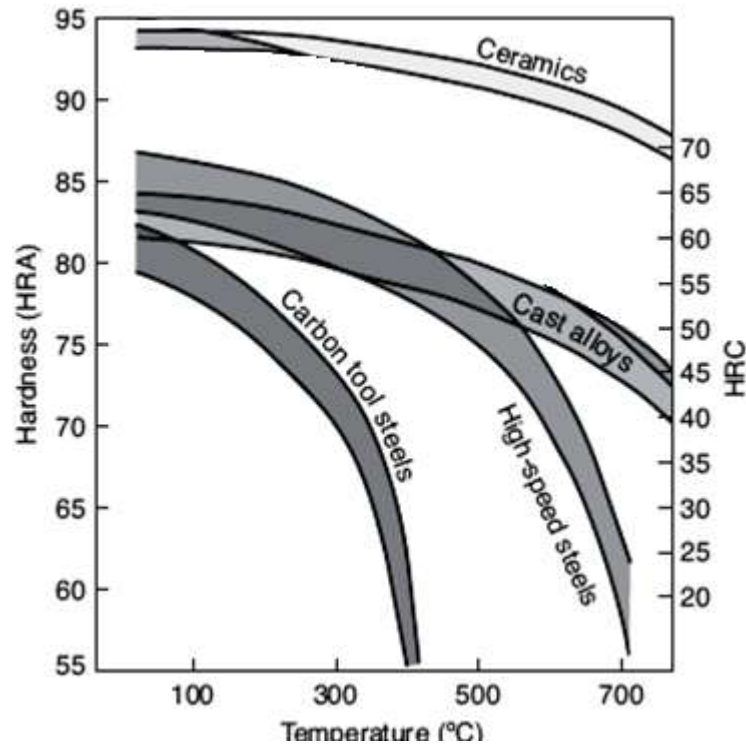


Fig. 1.2: Relationship between temperature and hardness for typical materials for cutting insert (Kalpakjian and Schmid, 2009).

Among of the popular candidate for cutting insert application is Al_2O_3 . Al_2O_3 based cutting inserts provide good abrasion resistance and its hot hardness is high. Chemically, cutting inserts made from Al_2O_3 are more inert than high speed steels and carbide inserts at elevated temperature. Besides their good mechanical properties, Al_2O_3 lack toughness, which makes the insert prematurely fail by chipping during machining.

Despite their weaknesses, these brittle Al_2O_3 based cutting insert still can be used in machining. However, their application is limited. In order to avoid premature failure or chipping, the lathe or CNC machine selected for machining must have minimum vibration ($< 0.28 \text{ mm/sec (RMS)}$), according to ISO 2372 – Vibration Severity Standard. Furthermore, these brittle cutting insert should only be use to machine soft material, such as aluminium metal. Optimization of the cutting force is critical in the

application of brittle cutting insert. Thus, the chosen cutting parameter (depth of cut, cutting speed and feed rate) must result minimum force on the insert.

However, this weakness can be overcome by adding secondary material like Y_2O_3 stabilized ZrO_2 (YSZ). With the introduction of few mechanisms to enhance toughness, Al_2O_3 based cutting insert with YSZ reinforcement has proven to be one of the promising cutting inserts (Kalpakjian and Schmid, 2009).

ZTA ceramic composites have been an interesting subject of research due to its high fracture toughness ($6 - 12 \text{ MPa.m}^{1/2}$), hardness ($\sim 1600 \text{ HV}$), high bulk density (4.1 g/cm^3) and chemical stability up until 1650°C . Previously mentioned properties have qualified cutting insert made from ZTA ceramic composite suitable for a cutting insert application (Du *et al.*, 2012; Faga *et al.*, 2012).

1.2 Problem statement

The disadvantages of ZTA is that a portion of Al_2O_3 is substitute out for YSZ (Geuzens *et al.*, 2008; Oelgardt *et al.*, 2010; Li *et al.*, 2012; Ortmann *et al.*, 2012). Previous work done by Azhar *et al.* (2009) showed that the Vickers hardness of Al_2O_3 reduces from 1810 HV to 1640 HV with the introduction of 20 wt % of YSZ. The reduction of Vickers hardness reduces the tool wear and the tool life (Medvedovski, 2001; Bitterlich *et al.*, 2008). The loss of Vickers hardness can be recovered by using additives. Previous work by Coble in 1961 proved that the introduction of MgO in Al_2O_3 matrix will result in a significant effect on the mechanical and electrical properties of Al_2O_3 (Coble, 1961). Similar observations were also reported by other authors where as the presence of sintering additives can improve the properties of the sintered product (Wang *et al.*, 1998; Rittidech *et al.*,

2006; Ahangarkani *et al.*, 2012; Huang *et al.*, 2012; Rittidech and Tunkasiri, 2012; Song *et al.*, 2012; Rittidech *et al.*).

Another factor that affects the efficiency of additives in the ceramic sintering process is particle size. Previous report by Golsa *et al.* (2007) have shown that the effect of additive's particles sizes such as talc and boehmite in Al_2TiO_5 ceramic system increased the bulk density. The increasing of bulk density on different system of materials were also reported by other researchers as well (Fu *et al.*, 1994; Jeong and Niihara, 1997; Lumley and Schaffer, 1998; Nawa *et al.*, 1998; Rice, 2000; Ji and Yeomans, 2002; Homaeigohar *et al.*, 2006). Furthermore, with recent advancement of materials, addition of nanomaterials has shown to have significant effect on bulk density and mechanical properties (Wu *et al.*, 2004; Jang, 2005; Ko *et al.*, 2005).

Besides hardness, fracture toughness is also one of the important characteristics for a cutting insert to perform without experiencing premature failure (Kalpakjian and Schmid, 2009). Cutting insert with low toughness often failed early during the machining process (Ezugwu and Wallbank, 1987; Dudzinski *et al.*, 2004). For ZTA ceramic composite, the toughness can be improved by increasing the content of YSZ. However, previous study has shown that reducing Al_2O_3 content would decrease the hardness since Al_2O_3 is traded out and replaced by YSZ (Cesari *et al.*, 2006; Azhar *et al.*, 2009). Alternatively, introduction of additives can be used to improve the composite's fracture toughness. Previous research has shown that the fracture toughness of Al_2O_3 -based ceramic composite can be improved by using additives such as CeO or Cr_2O_3 (Tien *et al.*, 1986; Zhang *et al.*, 1997; Riu *et al.*, 2000; Senthil Kumar *et al.*, 2004b; Magnani and Brillante, 2005; Senthil Kumar *et al.*, 2007; Yang *et al.*, 2012).

1.3 Research objectives

The objectives of this study are as follows:

- i. To investigate the effect of MgO additive on the mechanical properties and tool wear of ZTA ceramic composites.
- ii. To investigate the effect of MgO particles sizes as an additives on the mechanical properties and tool wear of ZTA ceramic composites.
- iii. To investigate the effect of Cr₂O₃ additive on the mechanical properties and tool wear of ZTA and ZTA-MgO ceramic composites.

1.4 Project approach

The study is divided into three parts. The Part 1 is to study the effect of MgO additive on the mechanical properties of ZTA ceramic composite. Samples with an 80/20 ratio for Al₂O₃/YSZ were prepared with different MgO wt% ranging from 0 wt% to 3.5 wt%. The samples were pressed at 300 MPa and subsequently sintered at 1600 °C for 4 hours. Vickers hardness (HV) and fracture toughness (K_{Ic}) were determined by Vickers indentation with a 30 kgf load. Field emission scanning electron microscopy (FESEM) was employed to study the samples microstructure. The samples were thermally etched in the same furnace used for sintering at 1400 °C for 2 hours. Machining test was done using a conventional lathe (Harrison 600) on commercially available stainless steel 316L.

Part 2 is to study the effect of MgO particle sizes as additive on the mechanical properties of ZTA ceramic composite. MgO in average particle sizes of 20 nm (Strem Chemicals), 100 nm (Alfa Aesar), 500 nm (Alfa Aesar) and 7000 nm (Alfa

Aesar) were added to the $\text{Al}_2\text{O}_3/\text{YSZ}$, respectively. The 80 % Al_2O_3 and 20 % YSZ samples were prepared with different MgO particle sizes and wt % ranging from 0.4 wt % to 0.9 wt.% for micron size of additives and 0.4 wt.% to 1.3 wt % for nano additive. The sample preparations and characterization techniques are identical to Part 1.

Part 3 is to study the effect of Cr_2O_3 additives on the mechanical properties of ZTA and ZTA-MgO ceramic composites. Samples with an 80/20 ratio for $\text{Al}_2\text{O}_3/\text{YSZ}$ and $\text{Al}_2\text{O}_3/\text{YSZ}/\text{MgO}$ were prepared with different Cr_2O_3 wt% ranging from 0 wt% to 1.0 wt%. Step for samples preparation and characterization techniques are similar to Part 1.

CHAPTER 2

LITERATURE REVIEW

2.1 Ceramic cutting insert

Ceramic cutting inserts were introduced in early 1950s, which consists of primarily fine grained, high purity aluminium oxide or alumina (Al_2O_3). They were pressed into inserts shapes at room temperature and with high pressure, sintered at high temperature and called white, or cold pressed ceramics (Kalpakjian and Schmid, 2009).

Al_2O_3 -base ceramic inserts shows high abrasion resistance and high hot hardness (Fu *et al.*, 1994). They are chemically more stable than cutting insert made from high speed steels and carbides. Good surface finish is also obtained with ceramic inserts in cutting cast irons and steels. Unfortunately, ceramics especially Al_2O_3 lack toughness which leads to premature insert failure by chipping (Kalpakjikan and Schmid, 2003).

Previous work by Trent and Wright (2000) also reported that Al_2O_3 is one of refractory oxides which shows high hardness and melting point. Disposable cutting insert consisting of almost 100% Al_2O_3 has been commercially available for more than 30 years and have been used in many countries for machining steel and cast iron.

Nowadays, an extensive series of types of ceramics are currently being applied and developed as cutting inserts, including Al_2O_3 , $\text{Al}_2\text{O}_3/\text{ZrO}_2$, SiC whiskers reinforced Al_2O_3 , $\text{Al}_2\text{O}_3/\text{TiC}$ and Si_3N_4 composites. Furthermore, microstructures are being optimized for high strength, toughness and hardness (D'Errico *et al.*, 1999).

2.2 Al₂O₃ as a cutting insert

Al₂O₃ is used in many kind of abrasive wear environment such as coal chutes, ball mills, dies, grinders, mixers, containers for abrasive slurries and cutting inserts (Dogan and Hawk, 1997; Bernardi *et al.*, 2004). Al₂O₃ offer advantages such as high hot hardness, high abrasion resistant, chemically inert and relatively cheap. Table 2.1 shows the mechanical properties of Al₂O₃ which makes it one of the most popular materials chosen for metal cutting applications.

Table 2.1: Mechanical properties of Al₂O₃ (Al-Naib, 2000).

Properties	Values
Density (g/cm ³)	3.96
Poisson ratio	0.2
Elastic modulus (Gpa)	400
Flexural strength (Mpa)	340
Vickers hardness (HV)	1900
Fracture toughness (Mpa.m ^{1/2})	4.0

2.3 Disadvantages of Al₂O₃ as a cutting insert

In spite of the variety of useful physical properties of sintered oxide ceramics based on chemically and thermally stable modification of α -Al₂O₃, their application as cutting tool inserts working under mechanical loads and thermal shock conditions is limited due to their brittleness and low strength. To overcome the brittleness, reinforcement such as YSZ is introduced into Al₂O₃. YSZ increases the toughness by the phase transformation from ZrO_{2(t)} to ZrO_{2(m)} (Dogan and Hawk, 1997; Smuk *et al.*, 2003; Szutkowska, 2004).

Even with modern and advanced processing, the brittleness of monolithic Al₂O₃ is still a critical weakness (Xu *et al.*, 2001). To overcome this problem, efforts have been made by reinforcing Al₂O₃ with SiC whiskers and ZrO₂ particles.

2.4 Yttria stabilized zirconia (YSZ)

Zirconium dioxide (ZrO_2), widely known as zirconia, is a white crystalline oxide of zirconium. Its most naturally occurring form, with a monoclinic crystalline structure, is the rare mineral, baddeleyite. The high temperature cubic crystalline form, called 'cubic zirconia', is rarely, if ever, found in nature, but is synthesized in various colours for use as a gemstone (Basu *et al.*, 2004a).

Zirconia is one of the most studied ceramic materials. Pure ZrO_2 has a monoclinic crystal structure at room temperature and transforms to tetragonal and cubic at increasing temperatures. The volume expansion ($\sim 4\%$) caused by the cubic to tetragonal to monoclinic transformations induce very large stresses, and will cause pure ZrO_2 to crack upon cooling from high temperatures. Several different oxides are added to zirconia to stabilize the tetragonal and/or cubic phase: magnesium oxide (MgO), yttrium oxide (Y_2O_3), calcium oxide (CaO), and cerium oxide (Ce_2O_3), amongst others (Basu, 2005).

In zirconia containing ceramics, maximum toughness can be achieved by manipulating the advantage of tetragonal-to-monoclinic martensitic transformation that can be induced in the stress field of an approaching crack. Much research has focused on the mechanisms of 'transformation toughening' in zirconia (Dogan and Hawk, 1997; Mishra *et al.*, 1998). Dogan and Hawk (1999) also reported that materials in which zirconia are added as a reinforcement phase may be toughened and strengthened by any one, or combination of the following mechanisms:

- Transformation toughening
- Microcracking at monoclinic zirconia-matrix interfaces
- Crack deflection by zirconia particles

2.5 Zirconia toughened Al_2O_3 (ZTA)

Zirconia toughened Al_2O_3 (ZTA) has been reported to one of the most successful commercial ceramics based cutting inserts which fully utilized zirconia advantages (Maiti and Sil, 2011). Recently, materials with certain intermetallic matrices might also benefit from the addition of zirconia particles. Dogan and Hawk (1997) applied 20 mass % of zirconia into MoSi_2 system, which resulted in 25-100% increased of fracture toughness of the material, depending upon which toughening mechanisms are activated. Normally the tetragonal phase would transform into the monoclinic phase at low enough temperatures, but the high strength of the cubic phase prevents the required expansion from happening, freezing in the tetragonal precipitates. Monoclinic zirconia may also be present in the cubic grains and at the grain boundaries.

The toughening mechanism comes into play when a crack is encountered. The cubic grains are constraining the tetragonal precipitates that want to expand and release associated energy. When these grains are faced with a propagating crack tip, the tetragonal phase is released and allowed to change back to the more stable monoclinic phase. This results in the associated volumetric expansion, effectively closing the advancing crack.

Because strength increases linearly with the amount of tetragonal phase, zirconia with 100 % of tetragonal phase gives the highest strength. In addition, zirconia with 100 % phase of tetragonal is known as tetragonal zirconia polycrystals (TZP). The amount of added oxide must be limited (3 mol % - 12 mol %) so that the phase is still tetragonal during sintering (Llorca *et al.*, 2004). On the other hand, the amount must be not too small because then the transformation of the tetragonal grains to the monoclinic state could not be suppressed (Basu *et al.*, 2004b).

TZP is having the highest strength and fracture toughness. TZP is not only applicable in bulk form, but also as reinforcement in other ceramics. Fig. 2.1 shows Al_2O_3 reinforced with zirconia particles thus called ZTA. If the size of zirconia particles is larger than the critical value or if the compressive stresses during cooling are not sufficient, the phase transformation can occur during cooling resulting in no transformation toughening. Besides, another strengthening mechanism such as crack deflection and microcracking may be possible to occur (Basu, 2005). Once the transformation toughening occur, ZTA ceramic composite are no longer protected by the transformation toughening and expected to fail with further stress or load.

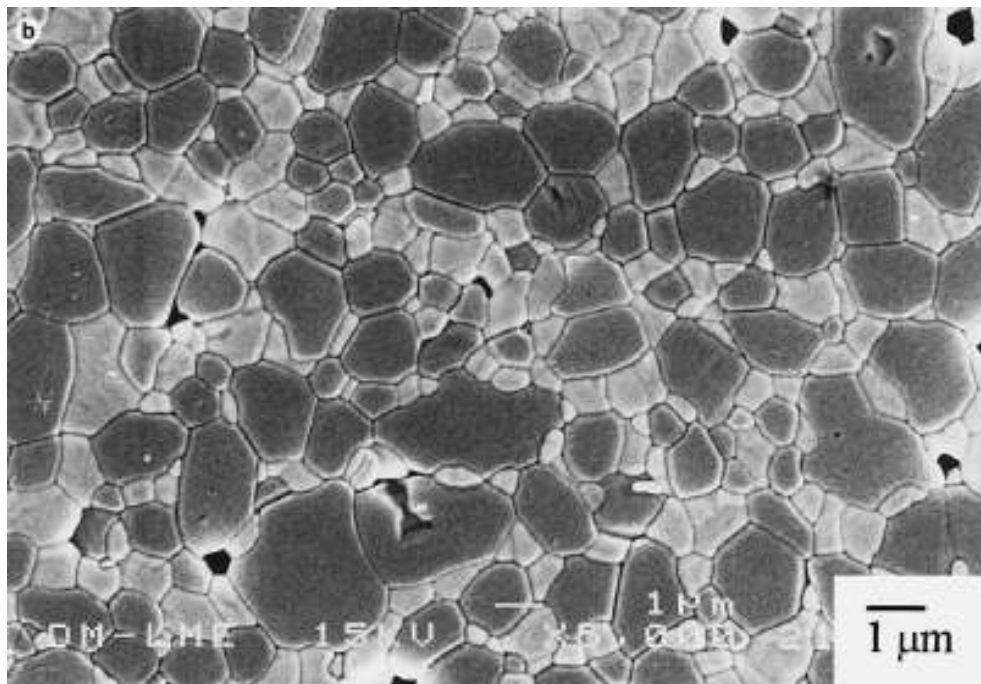


Fig. 2.1: Grain structure of zirconium oxide (light grey) in aluminium oxide (dark-grey). The horizontal bar has a length of 1 micron (Casellas *et al.*, 1999).

ZTA ceramic composite consists of Al_2O_3 as the matrix and ZrO_2 particle embedded inside it, either unstabilized or stabilized. Unstabilized ZrO_2 refer to ZrO_2 without the

presence of any stabilizer content and stabilized ZrO_2 refer to ZrO_2 with the presence of stabilizer such as MgO , Y_2O_3 and CaO . The addition of second phase is aimed for the enhancement of flexural strength, fracture toughness and fatigue resistance, mainly attributed to the stress-induced phase transformation of the tetragonal ZrO_2 which transforms into a more stable monoclinic phase. This transformation contributes to a volume increase of $\sim 4\%$ which induces compressive stress around a propagating crack and develops the toughening effect (Casellas *et al.*, 2003). Value of fracture toughness for ZTA ranging from $6 - 12 \text{ MPa}\cdot\text{m}^{1/2}$, showing a significant increase compared fracture toughness of Al_2O_3 ($3 \text{ MPa}\cdot\text{m}^{1/2}$). In terms of microstructure, ZTA micrograph show to have less amount of porosity compare to monolithic Al_2O_3 . Fig. 2.2 shows the micrograph for monolithic Al_2O_3 and ZTA.

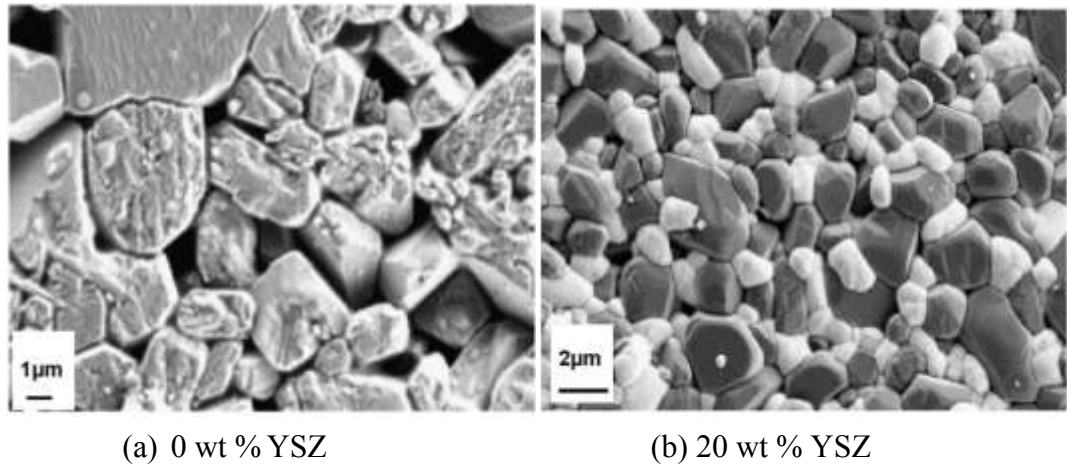


Fig. 2.2: Micrograph for (a) monolithic Al_2O_3 and (b) 80 wt % Al_2O_3 /20 % YSZ (Azhar *et al.*, 2009).

2.6 Fabrication method

Smuk *et al.* (2003) fabricated the ZTA cutting insert by pressing the mixture at 300 MPa. The samples were sintered in a high temperature electrical furnace with constant speed of heating and cooling rate, at temperature 1600°C . Smuk *et al.* (2003) also concluded that ZTA ceramic composite with 20 wt % of YSZ are

characterized to have the best mechanical properties from among the tested compound compositions.

Work done by Azhar *et al.* (2009) and (Hao *et al.*, 2010) used similar processing route. Monolithic Al₂O₃ and YSZ were mixed using a ball mill for 8 hours and hydraulically pressed at 300 MPa into a rhombic with an 80° angle cutting insert. The samples were later sintered at 1600 °C for 4 hours with 5°C/min sintering rate.

2.6.1 Sintering

Sintering is known as a process to create objects from powders or particles. The basic mechanism is atomic diffusion. Atomic diffusion occurs much faster at higher temperature. Few parameters are known to affect sintering such as type of materials, particle sizes, sintering atmosphere, temperature, time and heating rate (Rahaman, 2003).

There are 3 stages during sintering; starting, intermediate and finish. Fig. 2.3 shows the respective stages. During adhesion stage the particles comes into contact each other but do not form any bond. At initial stage, there is a rapid growth of the interparticle neck between the particles. At intermediate stage the pore structure becomes smooth (reach equilibrium shape) and develops interconnected particles. The intermediate stage usually covers the major part of the sintering process. Particles start to form grain boundaries. At the final stage, the densification process is stopped and the pores become spherical and separated (Rahaman, 2003).

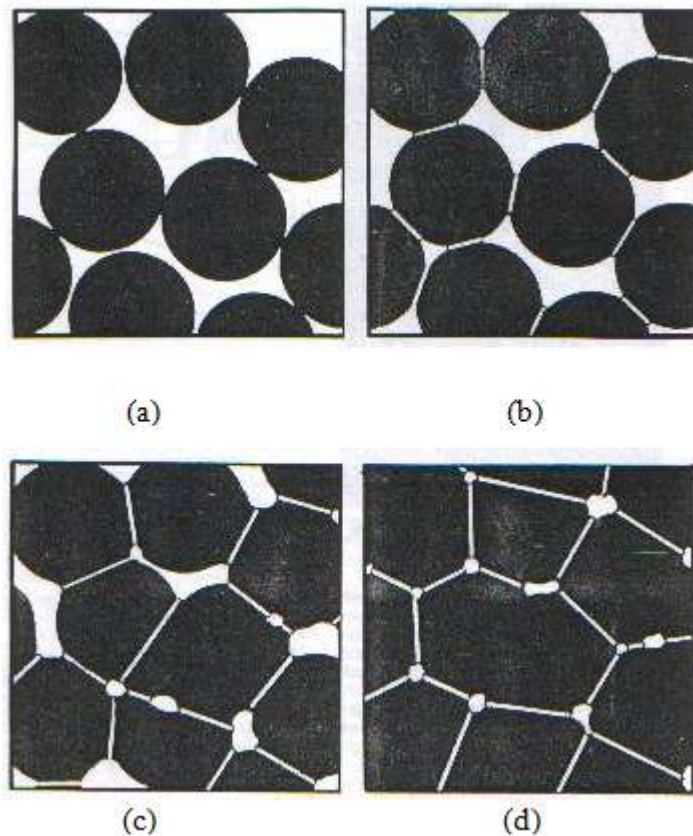


Fig. 2.3: Stages of sintering (a) free particles, (b) necking between particles, (c) formation of grain boundary, and (d) densification process and pores elimination (Randal, 1991).

Sintering occurs by diffusion of atoms through the microstructure. This diffusion is caused by a gradient of chemical potential-atoms that move from an area of higher chemical potential to an area of lower chemical potential. The different paths that the atoms take to get from one spot to another are known as the sintering mechanisms.

The six common mechanisms are:

- Surface diffusion – diffusion of atoms along the surface of a particle
- Vapor transport – evaporation of atoms which condense on a different surface
- Lattice diffusion from surface – atoms from surface diffuse through lattice
- Lattice diffusion from grain boundary – atom from grain boundary diffuses through lattice
- Grain boundary diffusion – atoms diffuse along grain boundary
- Plastic deformation – dislocation motion causes flow of matter

2.7 Effect of additives

2.7.1 Effect of MgO addition to Al_2O_3

Research done by Coble (1961) stated that small addition (≤ 0.25 wt %) of MgO would hinder the grain growth of Al_2O_3 during sintering process. In addition, Al_2O_3 with near theoretical density is possible with the addition of MgO (Ikegami *et al.*, 2010). Fig. 2.4 shows the densification of Al_2O_3 compacts with and without the addition of MgO. Al_2O_3 containing MgO (represents by solid circle) is shown to achieve 100% relative density while Al_2O_3 without MgO reaches 97% of relative density under the similar sintering condition. The work done by Coble (1961) suggests that the discontinuous grain growth of Al_2O_3 has been averted by the enhancement of the sintering rate by the presence of MgO.

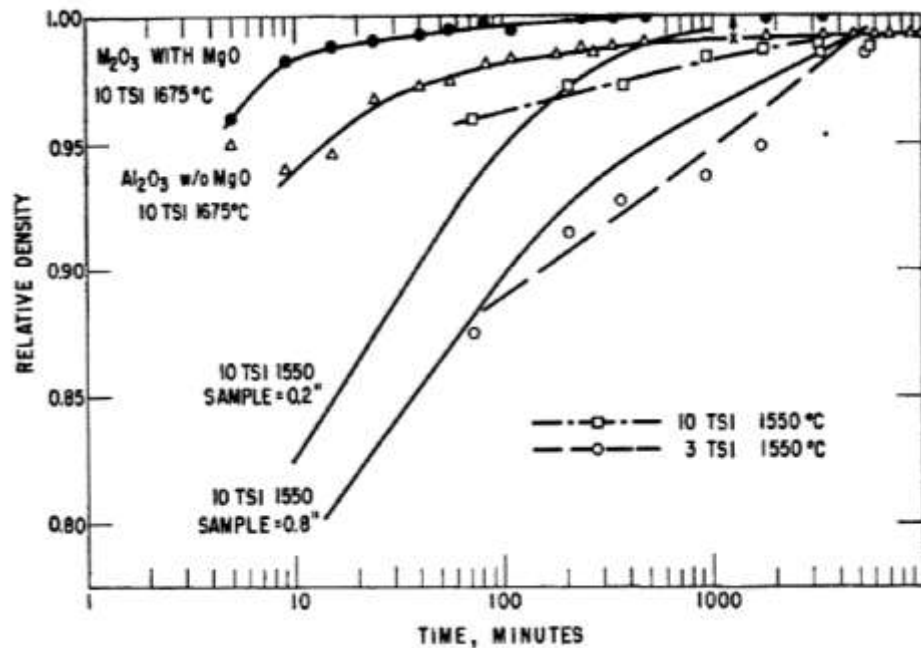


Fig. 2.4: Densification of Al_2O_3 compacts with and without MgO additives. TSI stands for tons per square inch (Coble, 1961).

Fig. 2.5 shows the grain growth of Al_2O_3 compacts with different temperature and additives as variables. One series containing Al_2O_3 with 0.25 wt % of MgO and is shown by filled circles while Al_2O_3 without MgO is represented by open diamonds.

Both Al_2O_3 series shows normal grain growth up to a size of $10\ \mu\text{m}$ at 560 min. Beyond 560 min, Al_2O_3 with MgO continue to exhibit normal growth, while undoped Al_2O_3 samples undergo discontinuous grain growth. According to Coble (1961) at 1800 min the discontinuous growth is completed and the undoped Al_2O_3 samples show final grain size of $208\ \mu\text{m}$. Beyond 1800 min, grain size for Al_2O_3 doped with MgO was observed does not to decrease lower than $130\ \mu\text{m}$.

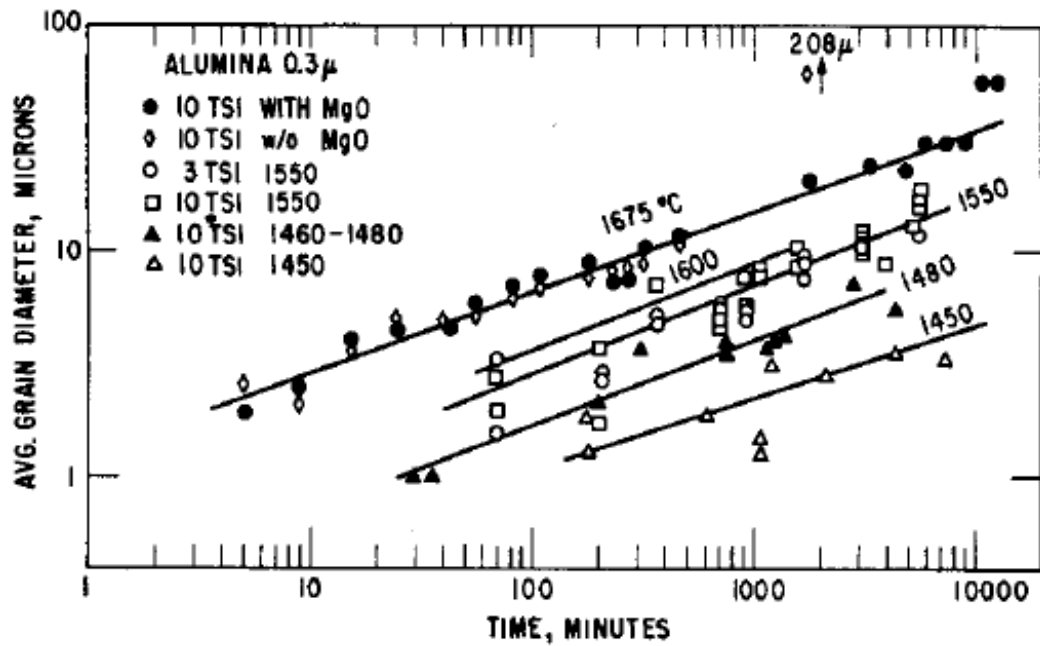


Fig. 2.5: Grain growth in Al_2O_3 compacts with temperature, forming pressure and magnesia additives as variables (Coble, 1961).

Explanation by Rahaman (2003) showed that the addition of MgO would decrease the grain mobility in Al_2O_3 . Two mechanisms have been proposed i.e. (i) solute drag due to Mg^{2+} segregation at grain boundaries, and (ii) pinning of the grain boundaries by fine particles of MgAl_2O_4 . However, use of MgO with another additives material will mask the effect of MgO on Al_2O_3 .

A study by Rittidech *et al.* (2006) also highlighted the potential of MgO as sintering additives for Al_2O_3 . Addition of MgO would result in a smaller grain size and decrease the fracture toughness significantly. In addition, MgO is one of the

additives that can be used to reduce the sintering temperature and enable to sinter Al_2O_3 to near theoretical density.

Fig. 2.6 shows the MgO – Al_2O_3 phase diagram use by Sarkar and Banerjee (1999) in his previous work. Sarkar and Banerjee (1999) studied the densification mechanism of MgO – Al_2O_3 compacts with MgO to Al_2O_3 molar ratios 1:1 (stoichiometric spinel), 2:1 (magnesia rich spinel) and 1:2 (alumina rich spinel). They found that very high density can be obtained in a single stage sintering process for all the stoichiometric and nonstoichiometric spinels (MgO : Al_2O_3 molar ratios=2:1, 1:1 and 1:2) by incorporation of milling process.

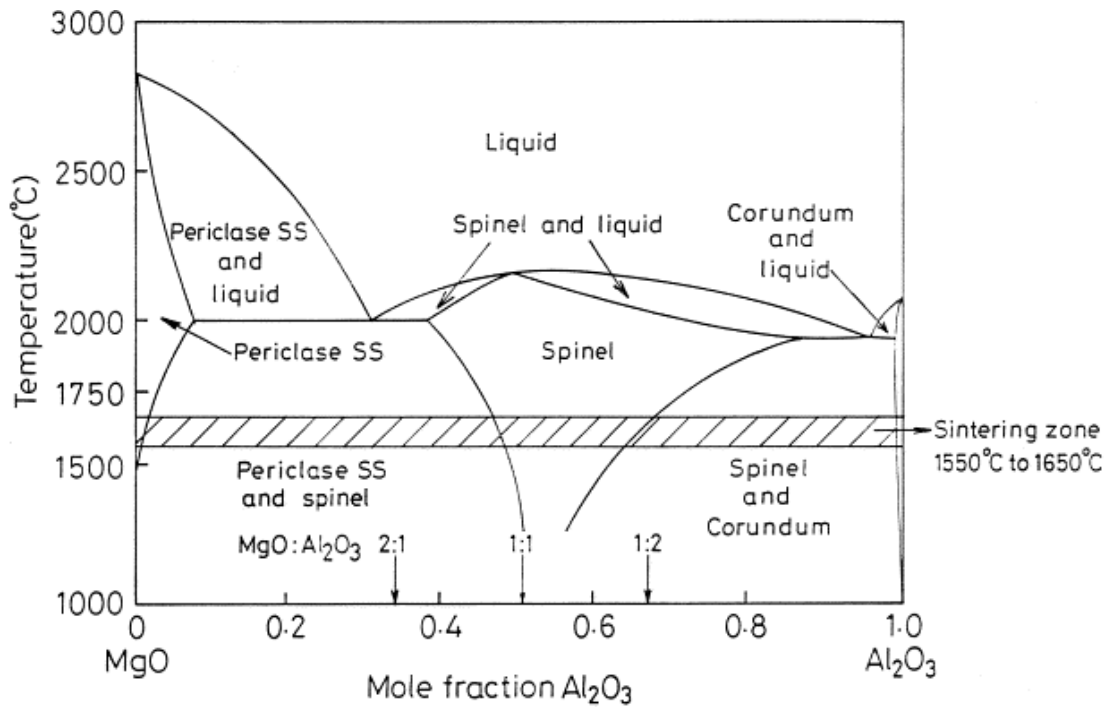


Fig. 2.6: Phase diagram of the system MgO – Al_2O_3 (Sarkar and Banerjee, 1999).

Previous work by Greskovich and Brewer (2001) and Miller *et al.* (2006) focused on determining the solubility limit of MgO in Al_2O_3 . Greskovich and Brewer (2001) conclude that the The solubility limits of MgO in Al_2O_3 were very low (~75 ppm

MgO at 1720°C and 175 ppm MgO at 1880°C). Miller *et al.* (2006) reported that the solubility limit of MgO in Al₂O₃ at 1600°C was found to be 132±11 ppm.

2.7.2 Effect of Cr₂O₃ addition to Al₂O₃

Similar with other ceramics, the strength of Al₂O₃ is proportional to the size of its grains. High strength as well as high hardness is obtained when the grain size is fine and homogeneous. However, the fracture toughness is generally low if the grain is small and homogeneous. Therefore, the fracture toughness will be increased when there are large elongated or platelike grains dispersed in a fine-grained matrix. This is because large grains can resist crack propagation in a fracture process (Riu *et al.*, 2000).

Previous research done by Hirata *et al.* (2000) showed that the addition of Cr₂O₃ would increase the fracture toughness of Al₂O₃. When Cr₂O₃ is added into Al₂O₃ system, isovalent solid solution will form over the full range of compositions due to both Cr₂O₃ and Al₂O₃ having the same corundum crystal structure. Reaction at high temperature (T >1000 °C) will produced a complete ranges of substitution solid solution (Magnani and Brillante, 2005). Isovalent solid solution happened when an atom or ion replaces an atom or ion of the same charge in the parent structure. It contributes to high refractoriness and chemical stability. The addition of Cr₂O₃ also increases the hardness, tensile strength and thermal shock resistance of Al₂O₃ (Riu *et al.*, 2000).

Based on Fig. 2.7, when a small amount of Cr₂O₃ (~2 mol %) was added, the grains became larger and bimodal in size distribution. Meanwhile, the fracture toughness and flaw tolerance of Al₂O₃ were improved. The hardness as well as elastic modulus was increased. However, fracture strength decreased by the Cr₂O₃ additions. The

large grains had platelike shape and were composed of a core region that is free from Cr^{3+} and a surrounding shell region rich in Cr^{3+} (Riu *et al.*, 2000).

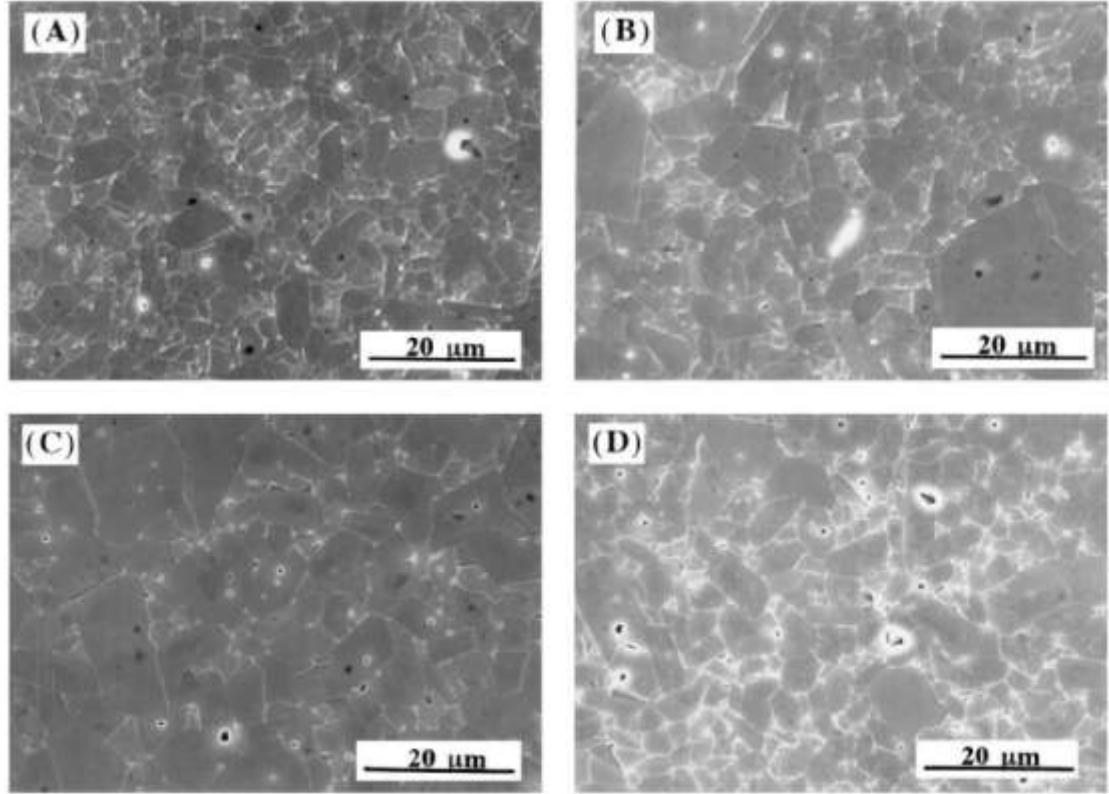


Fig. 2.7: Morphologies of Al_2O_3 specimens hot pressed at 1500°C for 1 h containing (A) 0 mol%, (B) 2 mol%, (C) 5 mol%, and (D) 10 mol% of Cr_2O_3 (Riu *et al.*, 2000).

The increase of Al_2O_3 grains size is due to the presence of Cr^{3+} ions. Diffusion of Cr through Al_2O_3 surface is faster compared to bulk diffusion. As a result, Al_2O_3 grains adjacent to Cr_2O_3 become full with Cr^{3+} ion during sintering. Those grains show faster grain growth. Riu *et al.* (2000) mentioned that large grains of Al_2O_3 will produce a platelike morphology as shown in Fig. 2.8. The formation of platelike grains was previously reported to increase the fracture toughness (Riu *et al.*, 2000; Magnani and Brillante, 2005).

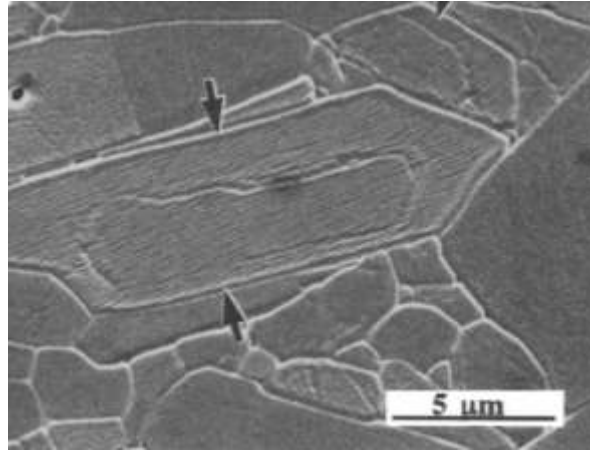


Fig. 2.8: Morphology of platelike grains, shown by the arrow in the figure (Riu *et al.*, 2000).

Table 2.2 shows the mechanical properties Al_2O_3 added with different amount of Cr_2O_3 . Based on the Table 2.2, Al_2O_3 added with 2 mol% produced the highest fracture toughness, modulus of rupture as well as microhardness values. Value of Vickers hardness increased from $1681 \text{ HV} \pm 20$ to $1738 \text{ HV} \pm 26$ with 2 wt % of Cr_2O_3 . However with further amount of Cr_2O_3 , the value of Vickers hardness decreases. The author stated that it may cause by the presence of large Al_2O_3 grain size in the ceramic composite (Riu *et al.*, 2000). In this study, the fracture toughness reference value used for monolithic Al_2O_3 and ZTA is $2.98 \text{ MPa}\cdot\text{m}^{1/2}$ and $5.93 \text{ MPa}\cdot\text{m}^{1/2}$, respectively.

Table 2.2: Summary of mechanical properties of Al_2O_3 contain different amount of Cr_2O_3 (Riu *et al.*, 2000).

Cr_2O_3 mol %	K_{IC} ($\text{MPa}\cdot\text{m}^{1/2}$)	K_{IC} %	MOR (MPa)	E (GPa)	HV (kg/mm^2)	HV %
0	3.7	0	445	407	1681	0
2	4.7	27	355	411	1738	3.0
3	4.5	21	386	412	1714	2.0
5	3.9	5	350	402	1653	-1.6

Research done by Magnani *et al.* (2005) showed that the fracture toughness of ZTA system can be improved with addition of small amount of Cr_2O_3 . Fracture toughness of ZTA system has increased 12.3% with addition of 0.5wt% of Cr_2O_3 .

Study by Hirata *et al.* (2000) showed that Cr_2O_3 and Al_2O_3 forms solid solution over the complete range of composition as shown in Fig.2.9. At 1200°C , Cr_2O_3 is not stable and prone to become CrO_3 . The CrO_3 is produced at high vapour pressure. It is hard to obtain a high density of Cr_2O_3 via solid state sintering. By sintering Cr_2O_3 in a control environment (vacuum or in an inert gas atmosphere), the relative density can be increased. Al-Douri *et al.* (1994) and Yamauchi *et al.* (2003) reported that the evaporation of Cr_2O_3 in O_2 atmosphere is caused by the following reaction:

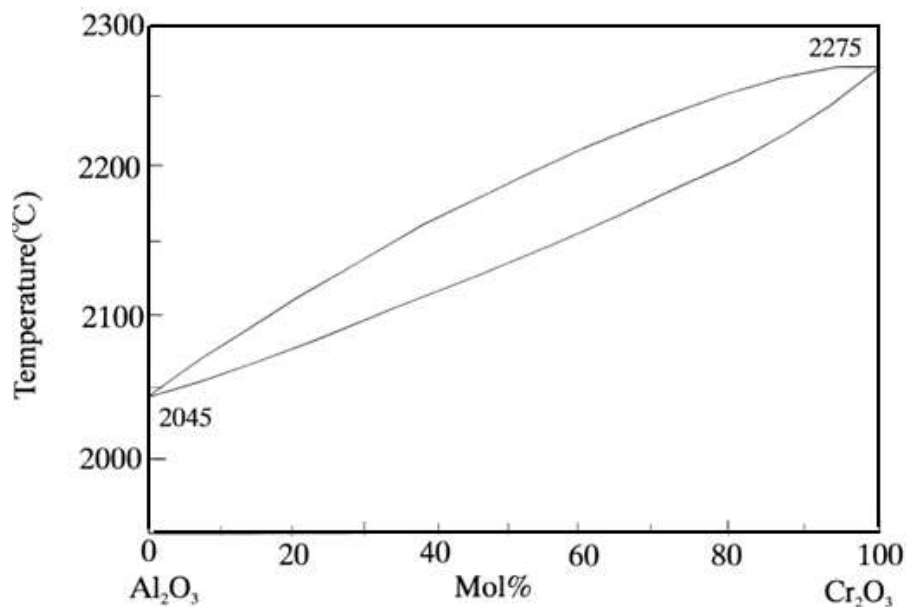


Fig.2.9: Phase relationship between Al_2O_3 - Cr_2O_3 (Hirata *et al.*, 2000).

2.8 Effect of particle size and grain size on mechanical properties

Studies done by Teng *et al.* (2007) showed the effect of Al_2O_3 particle size on the mechanical properties of alumina-based ceramics. By comparing the monolithic nano-scale alumina ceramics and monolithic micro-scale alumina ceramics, the monolithic nano-scale alumina ceramics showed intergranular fracture mode and higher flexural strength due to finer grain and higher density. The mechanical properties of the $\text{Al}_2\text{O}_{3\mu}/\text{Al}_2\text{O}_{3n}/\text{SiC}_n$ multi-scale nanocomposite were also greatly improved. When hot-press fabricating nano-scale Al_2O_3 particles and nano-scale SiC particles at 1700 °C, these particles can form homogeneous and compact body. When observing the microstructure, the grain boundary of the composite is reinforced thus resulting in the transition from intergranular to transgranular fracture mode. The $\text{Al}_2\text{O}_{3\mu}/\text{Al}_2\text{O}_{3n}/\text{SiC}_n$ composite had higher mechanical properties than $\text{Al}_2\text{O}_{3\mu}/\text{SiC}_n$ composite due to the size matched effect and the different thermal expansion coefficient of the nano-scale Al_2O_3 particles.

Many researchers (Hall *et al.*, 1995; Goh *et al.*, 1997; Azhar *et al.*, 2009; Jianxin *et al.*, 2009; Xu *et al.*, 2009; Zhao *et al.*, 2010) have done their investigation on the wear resistance of alumina ceramic by focusing on the microstructure and alumina grain size. They found that by reducing the matrix grain size and promoting narrow grain size distribution; this method can enhance the wear resistance of the material in abrasive and sliding environments. Besides that, porosity has also been shown to affect the wear behaviour of alumina ceramics. Increase in porosity will lead to a decrease in wear resistance.

The mechanical properties of ceramics are often dependent on the grain size of the materials. Materials with fine-grained size ($< 10\mu\text{m}$) usually have superior properties. Cutting insert with long life requires grain size less than $3\mu\text{m}$, uniform

grain size and minimum porosity. Besides that, inserts with smaller average and uniform grain size showed a longer tool life and machinability.

Dogan and Hawk (1999) also suggested that the microstructure and overall chemistry of the ceramic must be taken into consideration when selecting a high-alumina material for a wear-resistant application. In order to optimize the abrasive wear-resistance, the alumina grain size must be small, regardless of the alumina content. Besides that, if second phases are present at the boundaries, they should be amorphous and with composition high in alkaline earth constituents to reduce their softening point.

Study was also done by Ko *et al.* (2005) on the Al_2O_3 -SiC composite system containing 30 wt % of dispersed SiC particles ($\sim 280\text{nm}$) which was fabricated through hot-pressing and machined as cutting inserts. The Al_2O_3 -SiC particulate composites exhibit higher hardness than the unreinforced matrix. This is because the SiC inhibits grain growth and the SiC is present as the hard secondary phase. The SiC particles on the grain boundary of the composites contribute to the increasing of toughness at high SiC loadings ($\geq 20\text{wt.}\%$). The reduced grain size and the transformation of the fracture mode from intergranular to intragranular of the composite lead to the reduction of the fracture toughness whereas crack deflection by the SiC particles contributed the increase in toughness.

2.9 Effect of mechanical properties on tool wear

In cutting insert application, hardness and fracture toughness are the main mechanical properties that will affect the wear behaviour of the insert. The role of hardness is to resist wear during machining against the workpiece. Theoretically, cutting insert with high hardness will have longer tool life due to its high wear